

## ON THE INCLUSION OF THREE-DIMENSIONAL EFFECTS IN SIMULATIONS OF TWO-DIMENSIONAL BLUFF-BODY WAKE FLOWS

R. Mittal†

Center for Turbulence Research

Stanford University

Stanford, California, 94305

S. Balachandar

Department of Theoretical and Applied Mechanics

University of Illinois at Urbana-Champaign

Urbana, Illinois 61801

### ABSTRACT

Unsteady flow past a circular cylinder at a Reynolds number of 300 has been simulated. The spanwise extent of the computational domain has been systematically varied from zero (2-D) to a large value of  $12\lambda_z$ , where  $\lambda_z$  is the spanwise wavelength of the fundamental mode-B 3-D instability (Williamson, 1996). Simulations with intermediate spanwise extent of  $\lambda_z$  and  $2\lambda_z$  have also been performed so as to isolate the role of mode-B instability, its spanwise subharmonic instability and other longer wavelength instabilities. The results suggest that while imprints of mode-B and its subharmonic instability can be observed in the near wake region, further subharmonic instabilities of larger wavelength are feasible downstream, leading to a rearrangement of the vortical structure and its spectral content. Furthermore, the prediction of global quantities such as lift and drag improves as the spanwise domain size is increased.

### INTRODUCTION

It has now been firmly established that beyond a certain range in Reynolds number, wakes of two-dimensional (2-D) bodies become susceptible to a primary three-dimensional (3-D) Floquet instability mechanism (Noack et al. 1993, Barkley & Henderson, 1996) which leads to the amplification of 3-D disturbances and eventual development of strong streamwise oriented vortical structures. The structure and evolution of these vortical structures has been studied in some detail in mixing layers (Moser & Rogers 1991), plane wakes (Meiburg & Lasheras, 1988), wakes of circular cylinders (Williamson, 1991, Karniadakis & Triantafyllou, 1992, Mittal & Balachandar, 1995a, Williams et al., 1996, Wu et al., 1994, Zhang et al. 1995)

†Current Address: Department of Mechanical Engineering,  
University of Florida, Gainesville, Florida 32611.

and elliptic cylinders (Mittal & Balachandar, 1994, Mittal 1995). It has been shown that these 3-D vortical disturbances alter the structure and evolution of the Karman vortices in the near wake (Mittal & Balachandar, 1995b) and as a result, 2-D simulations which do not allow for the existence of these streamwise vortices fail to accurately predict even gross quantities such mean drag and root mean square (r.m.s.) lift fluctuation.

Different modes of 3-D instability have been observed (Williamson 1996). At Reynolds numbers above a critical value for the onset of three-dimensionality, mode-A instability is observed with an approximate spanwise wavelength of about  $3.5D$  (Barkley & Henderson 1996) for the 3-D streamwise vortices, where  $D$  is the diameter of the cylinder. Above a slightly higher second critical Reynolds numbers, mode-B 3-D disturbance also becomes unstable and its spanwise wavelength is about  $D$ . For the case of circular cylinder, the critical Reynolds number for the onset of mode-A instability is about 188 and for the onset of mode-B instability is about 260. As Reynolds number is increased further, Karniadakis & Triantafyllou (1992) suggest that a sequence of period-doubling instabilities begin before  $Re=300$  and that the flow transitions to a chaotic state by  $Re=500$ . Recent simulations (Mittal & Balachandar, 1995b) and experiments (Williams et al. 1996) confirm the possibility of a subharmonic instability with a spanwise wavelength of twice the fundamental, resulting in a period-doubling bifurcation the flow involving  $1/2$  the fundamental Strouhal frequency. Experimental measurements show in addition to  $1/2$  subharmonic frequency,  $1/3$  and lower subharmonic frequencies as well (Williamson 1996) suggesting alternative routes to chaos in the wake. Owing to the limited spanwise extent employed, the results of the above simulations only confirmed that the mode-B primary 3-D disturbance is unstable to subsequent spanwise subharmonic

instability, but could not verify the possibility of other longer spanwise wavelength instabilities. Simulations in larger spanwise domains (Thompson et al. 1995) show a rather complex evolution of the wake.

In order to address some of these issues, here we consider the wake of a circular cylinder at a Reynolds number of 300. The spanwise extent of the computational domain has been systematically varied from zero (2-D) to a large value of  $12\lambda_z$ , where  $\lambda_z$  is the spanwise wavelength of the fundamental mode-B 3-D instability, chosen here to be  $0.9D$ . The two-dimensional simulation forms the limiting case where 3-D disturbances are completely eliminated. A second simulation has been performed with a spanwise domain of  $\lambda_z$  in order to isolate and examine the role of mode-B instability, which is the dominant primary 3-D instability at  $Re=300$ . A third simulation has been performed in a 3-D computational domain of spanwise extent  $2\lambda_z$ , which allows for a possible subharmonic instability. The large domain of  $12\lambda_z$  has been chosen in order to simultaneously accommodate mode-A, mode-B and subharmonic instabilities. Furthermore, the large spanwise domain will allow for their nonlinear interaction and any other possible long wavelength instability.

Most previous simulations, owing to computational limitations, have either chosen a well resolved computational domain of smaller spanwise extent or a large spanwise extent at a much lower resolution. All the results to be reported here, including the large computation of spanwise extent of  $12\lambda_z$ , were performed at very high resolution. The criterion employed is that each of the 3-D streamwise vortices be well resolved. In the largest domain of spanwise size  $12\lambda_z$  up to 24 streamwise vortices are observed in the near wake and with a spanwise resolution of 288 points, the compact-core of each of these vortices is well resolved with 12 Fourier modes. Thus the above sequence of well resolved simulations will allow us to isolate and investigate the role of three-dimensionality arising from mode-B primary 3-D instability, its subharmonic instability and other longer wavelength instabilities. It is anticipated that this approach will allow us to explain the observed complex behavior of the cylinder wake in terms of the different instabilities and their interaction. It is also the objective of this paper to assess the effect that these instabilities have on the prediction of gross quantities like mean drag and r.m.s. lift and on other important characteristics of the near wake.

## SIMULATIONS METHODOLOGY

A Fourier-Chebyshev spectral collocation method (Canuto et al. 1988) is used to simulate the flow in a body fitted elliptic cylindrical grid. The circumferential direction ( $\theta$ ) is intrinsically periodic and a Fourier expansion is used in that direction. An appropriate spanwise length,  $L_z$ , is chosen for the various simulations and the flow is assumed to be periodic in the spanwise direction ( $z$ ). This allows for the use of Fourier discretization along this direction. The wall-normal direction ( $r$ ) is non-periodic and therefore a Chebyshev expansion is used for

discretization. The infinite flow domain is truncated to a finite domain in the radial direction and the computational outer boundary lies at a distance of  $15D$  from the cylinder and non-reflecting boundary conditions are applied at the outflow boundary. A mixed boundary condition is also applied at the inflow boundary which allows the incoming uniform flow to adjust to the displacement effect of the body. A two-step, time-split method is employed to advance the solution in time through the advection-diffusion and pressure-correction steps. A homogeneous Neumann pressure boundary condition is used on the body in conjunction with a higher order intermediate velocity boundary condition. These boundary conditions satisfy no-penetration exactly and no-slip to  $O(\Delta t^3)$  accuracy on the cylinder surface where  $\Delta t$  is the time-step size. Details of the numerical method are given in Mittal & Balachandar (1996) and Mittal (1995).

This study will consider detailed comparison of the predictions from different simulations with varying spanwise extent. It is therefore critical to show that the results are independent of the grid resolution and the domain size in the  $r$ - $\theta$  plane. To this end, we have conducted a series of 2-D simulation of flow past a circular cylinder at  $Re=300$  in order to assess the effect of the grid on the computed flow. The results of this study are summarized in Table 1. Simulation-I, is the reference simulations and it employs a mesh of 81 points in the radial direction and 160 points in the circumferential direction. The outflow boundary is located at a distance of  $15D$  from the origin. Simulation-II has 50% more points in the circumferential direction but has the same radial resolution. Simulation-III on the other hand has 50% more grid points in the radial direction but retains the circumferential resolution of Simulation-I. In Simulation-IV, the outflow boundary distance is 50% larger than Simulation-I and the number of points in both the radial and circumferential directions are increased by 50% in order to maintain a resolution at least as good as the reference simulation. Thus comparison of the results obtained from Simulations-II, III and IV with the results of the reference simulation allows us to assess individually the effect of increased circumferential resolution, radial resolution and domain size respectively. Quantities such as Strouhal number, and r.m.s. lift are typically quite sensitive to the grid resolution and domain size (Karniadakis et al., 1992, Behr et al. 1994). Both these quantities and the mean drag have been tabulated and it can be observed that all of these key quantities show less than 1% variation among the various simulations. Therefore the reference 2-D simulation is clearly grid and domain independent. In addition to this, spanwise grid independence for the 3-D simulations can be inferred by monitoring the decay in the spanwise energy spectra of the flow variables. The spanwise energy spectra of velocity measured at key locations in the wake for the various 3-D simulations shows at least five orders of magnitude decay implying that the simulations are extremely well resolved in the

spanwise direction. The final  $81 \times 160$  grid used in the current simulations is shown in Figure 1.

**Table 1.** Results of the grid and domain dependence study.

Simulation	Grid ( $r \times \theta$ )	Domain Radius	St	Mean $C_D$	R.M.S. $C_L$
I	$81 \times 160$	15D	0.213	1.381	0.652
II	$81 \times 240$	15D	0.212	1.375	0.647
III	$121 \times 160$	15D	0.213	1.383	0.651
IV	$121 \times 240$	22.5D	0.212	1.379	0.647

In all of the current 3-D simulations, three-dimensionality is explicitly initiated by introducing small amplitude spanwise perturbation in the flow field for a very short time period. The 3-D perturbations are then allowed to evolve naturally till a saturated three-dimensional state is reached. Subsequently, the flow field is averaged over a number of shedding cycles in order to obtain the wall and near wake statistics. The parameters of the various simulations and the disturbances used are given in Table 2. In the table, the disturbance is characterized by the spanwise wavelengths that are included in the disturbance.

**Table 2.** Description of various simulations included in the current study.

Simulation	Resolution ( $r \times \theta \times z$ )	Extent of Span	Description
2D	$81 \times 160 \times 1$	$L_z = 0$	No 3-D Disturbance
3DF	$81 \times 160 \times 36$	$L_z = \lambda_z$	mode-B 3-D Only
3DFS	$81 \times 160 \times 72$	$L_z = 2\lambda_z$	mode-B + 1/2-Subharmonic
3DA	$81 \times 160 \times 288$	$L_z = 12\lambda_z$	mode-B + up to 1/12-Subharmonic

## RESULTS AND DISCUSSION

### Three-Dimensional Vortical Structures

Proper identification and extraction of vortical structures is important in understanding their origin and dynamics and there are a number of methods available for the visualization of 3-D vortical structures. We observe that for the 3-D flow field encountered in the near wake, identification through the magnitude of the imaginary part of the complex eigenvalue ( $\lambda_i$ ) of the velocity gradient tensor is an effective means of extracting vortical structures (Mittal, 1995). This approach has been suggested and used before by a number of researchers to identify vortex structures (Soria & Cantwell 1993, Dallmann et al. 1991). This method is frame invariant and identifies a "vortical structure" as a region of large vorticity where rotation dominates over strain thus correctly eliminating shear layers from consideration. Thus, vortical structures identified using this method correspond to circular

streamlines in planes perpendicular to the axis of the structures. In subsequent plots, vortical structures will be identified by isosurfaces corresponding to one value of  $\lambda_i$ .

Figure 2 shows an isosurface plot of the vortical structures observed in the simulation 3DF where the only three-dimensionality is in the form of mode-B instability. In this plot, top, side and bottom views are shown on only a sector of the whole computational domain in the  $r-\theta$  plane. Also for visualization purposes the plotted domain has been extended in the spanwise direction by factor two using periodicity along the  $z$  direction. Thus two pairs of mode-B streamwise vortices can be observed in these plots. Furthermore, in the side view, two contour levels of spanwise vorticity have also been plotted at one local spanwise cross-section in order to provide a visual reference for the vortical structures. In all the plots, the flow is from the left to right and the base of the cylinder can be observed on the left side of the plot.

In Figure 2, the side view shows the clockwise rotating Karman vortex (CR1) in the initial stages of its roll-up in the near wake of the cylinder. The attached counter-clockwise rotating Karman vortex (CCR1) is in a mature stage of its rollup and a thin shear layer connects it to the attached boundary layer. In addition to the two vortices in the near wake, a shed clockwise rotating vortex (CR2) can also be observed on the right side of the plots. Furthermore, four mode-B streamwise vortices (R1) are also observed in the region between the counter-clockwise vortex and CR2. The thick arrows indicate the direction of rotation of these streamwise vortices. It can be observed in the bottom view that the mean spacing between all the streamwise vortices is also not the same and it can be clearly observed in the bottom view at the upstream end of the streamwise vortices that they appear as two distinct pairs of counter-rotating streamwise vortices with the upper two and the lower two forming the two pairs. The bottom view also shows a distinct and well organized spanwise variation in the clockwise vortex. This variations is induced by the action of the streamwise vortices, which alternately stretch and compress the spanwise vortex along the spanwise direction. In regions of stretching, the strength of the spanwise vortex is increased and this leads to the formation of "bulges" and in regions of compression, the strength of the spanwise vortex is decreased and "valleys" are formed. Moser & Rogers (1991) observed a similar interaction between the streamwise and spanwise vortices in a temporally evolving mixing layer where the stretching due to the streamwise vortices leads to the formation of "cup" shaped structures of concentrated spanwise vorticity. For details on the process by which these mode-B streamwise vortices are periodically autogenerated in the near wake, the reader is referred to Mittal & Balachandar (1995c)

The stability of the mode-B three-dimensional vortex shedding in the wake to spanwise subharmonic instability is investigated in case 3DFS, where the spanwise extent of the computational domain has been extended to  $2\lambda_z$  and a small amplitude disturbance of spanwise wavelength  $2\lambda_z$  has been superposed on the saturated mode-B of simulation 3DF. Figure

3 shows a top view of the vortex structures observed in simulation 3DFS. This one view is sufficient for pointing out the effect of the subharmonic mode on the topology of the vortical structures. Here again the flow is from left to right and the trailing section of the cylinder can be seen at the extreme left of the figure. Based on the spanwise periodicity of the flow, it is clear that the most outstanding feature is the large “horseshoe” shaped structure which is formed due to the distortion of the clockwise rotating spanwise roller that has just shed from the upper shear layer. Similar horseshoe vortical structures have also been observed at a higher Reynolds number of 525 (Mittal & Balachandar, 1995a) and therefore seem to be characteristic signature of the spanwise subharmonic mode. Furthermore, just like in the higher Reynolds number case, the “horseshoe” vortices appear at the same spanwise location only every alternate shedding cycle corresponding to a period doubling mechanism. The streamwise stretching of the legs of the horseshoe vortices leads to the formation of two of the streamwise vortices. Furthermore, we also observe that the streamwise vortices are of unequal strength and the two “bulges” in the spanwise Karman vortices are also of disparate sizes. The generation and evolution of the horseshoe and the streamwise vortices seem to follow along the observation of Mittal & Balachandar (1995a) for  $Re=525$ .

Figure 4 shows the top, side and bottom views of the vortical structures observed in the large-span simulation 3DA. The flow is again from left to right. The top view reveals a highly complex topology of the vortical structures. It is observed that the subharmonic mode corresponding to twice the wavelength of the mode-B and half the fundamental frequency is not the only subharmonic mode. There is now energy in the other subharmonic modes of longer wavelength,  $3\lambda_z$ ,  $4\lambda_z$ , etc. as well. The non-linear interaction of these modes and their superharmonics is what leads to the complex evolution of the vortical structures in the near wake. This result is in agreement with the simulations of Thompson et al. (1995). It should however be pointed out that despite the presence of subharmonic modes other than the 1/2-subharmonic mode, a number of observations made for 3DFS still hold for 3DA. In particular, the top view shows the distinct bulge-valley pattern observed in the two other simulations. Furthermore, a number of horseshoe shaped structures can also be observed which form out of the distorted spanwise roller and these structure are stretched in the streamwise direction to form the next generation of streamwise vortices. It is also of interest to note that while many streamwise vortical structures can be observed in the near wake region close to the cylinder base on the left hand side of the figure, the streamwise vortices seem to rearrange and significantly decrease in number farther downstream. This possibly suggests that while mode-B and its 1/2-subharmonic mode are dominant in the near wake region, further subharmonic instabilities of larger wavelength are feasible downstream, leading to a rearrangement of the vortical structure and its spectral content. It is also quite clear that a high resolution grid, as the one employed here, is

necessary in order to faithfully simulate the complex vortex dynamics in the near wake region, but a progressively coarser resolution may be sufficient in the downstream direction.

#### Effect of Spanwise Domain Size on Key Features of the Flow

All of these simulations have been carried out to a statistically stationary state and the flow has been time averaged over a number of shedding cycles. The table below summarizes some key wall statistics from the various simulations: In the table below, the quantity in brackets represents the error from the reference experimental measurement (except r.m.s.  $C_L$ ). A clear trend emerges from the above table. First, even at this relatively low Reynolds number, the 2-D simulation does an unsatisfactory job of predicting these key quantities. Furthermore, the prediction of the simulation improves as the spanwise domain size is increased and the best predictions are obtained with the largest span, ie. simulation 3DA. It is also observed that r.m.s. value of lift is very sensitive to the spanwise box size and can be significantly over-predicted if a small spanwise domain size is used. Predicting the fluctuation level of the aerodynamic forces is of key importance in fluid-structure interaction problems. On the other hand, mean quantities (mean drag and mean base pressure coefficient) are predicted much more accurately and predictions to within engineering accuracy can be obtained with a small spanwise domain. It should be pointed out that even though the Strouhal number is predicted quite accurately, the mean drag and base pressure coefficient for simulation 3DA are still off by about 3% from the experiments and this could perhaps be due to the existence of long time scales in the the simulation with the long spanwise domain which requires that averages be accumulated over a very long time.

**Table 3.** Comparison of wall statistics for the various simulations. The reference value of various quantities have been underlined and % deviation from the reference value is shown in brackets. †Williamson (1996); ‡Wieselsberger (1922)

Simulation	St	Mean $C_D$	R.M.S. $C_L$	Mean Base $C_p$
2D	0.213 (5%)	1.38 (13%)	0.65 (71%)	-1.22 (27%)
3DF	0.210 (3%)	1.32 (8%)	0.51 (34%)	-1.10 (15%)
3DFS	0.207 (2%)	1.27 (4%)	0.41 (8%)	-1.04 (8%)
3DA	0.203 (0%)	1.26 (3%)	<u>0.38</u>	-0.99 (3%)
Expts.	<u>0.203</u> †	<u>1.22</u> ‡	-	<u>-0.96</u> †

The underlying cause for the inaccurate predictions of the mean drag and r.m.s. lift by 2-D simulations has been addressed by Mittal & Balachandar (1995b). There it has been shown that the 3-D structures extract energy out of the 2-D shedding motion.

This results in a reduction of the 2-D Reynolds stresses which in turn is responsible for the reduction in base suction pressure and mean drag. The higher unsteady lift force in the 2-D simulations have been shown to be due to the fact that the Karman vortices approach closer to the body than in 3-D simulations. This overall reasoning can be extended further to explain the relatively inaccurate prediction of the simulations with small spanwise box sizes. As shown in Figure 2, the topology of the vortical structures is relatively simple in simulation 3DF and the Karman rollers are only minimally distorted by the streamwise vortices. However, the inclusion of subharmonic mode in 3DFS results in the development of more complicated vortical structures including horseshoe shaped structures which are able to extract more energy from the 2-D vortex shedding motion. This results in a further reduction in the level of Reynolds stresses in the near wake with a corresponding reduction in the mean drag and r.m.s lift. The most complex topology is observed in simulation 3DA and again, this increased complexity is attained at the expense of the 2-D shedding motion and the computed solution is observed to approach even closer to the experiments.

#### ACKNOWLEDGEMENT

These computations have been performed on the Cray C-90 at the Pittsburgh Supercomputer Center.

#### REFERENCES

Barkley, D., and Henderson, R.D. 1996. Three dimensional Floquet stability analysis of the wake of a circular cylinder. Submitted to *J. Fluid Mech.* 322.

Behr M., Hastreiter, D., Mittal, S. and Tezduyar, T.E. 1994, Incompressible flow past a circular cylinder: Dependence of the computed flow field on the location of the lateral boundaries, Univ. of Minnesota Supercomputer Institute Research Report UMSI 94/189.

Canuto, C., Hussaini, M.Y., Quarteroni, A. and Zang, T.A. 1988, *Spectral Methods in Fluid Dynamics*, Springer-Verlag.

Dallmann, U., Hilgenstock, A., Riedelbauch, S., Schulte-Werning, B., and Vollmers, H. 1991. On the footprints of three-dimensional separated vortex flows around blunt bodies. *AGARD CP-494*.

Karniadakis, G. E., and Triantafyllou, G. E. 1992. Three-dimensional dynamics and transition to turbulence in the wake of bluff objects. *J. Fluid Mech.*, 238, 1-30.

Mansy, H., Yang, P-M and Williams, D. R. 1994. Quantitative measurements of three-dimensional structures in the wake of a circular cylinder. *J. Fluid Mech.*, 270, 277-296.

Meiburg, E., and Lasheras, J. C. 1988. Experimental and numerical investigation of the three-dimensional transition in a plane wake. *J. Fluid Mech.*, 190, 1-37.

Mittal, R. and Balachandar, S. , 1994. Study of Flow Over an Elliptic Cylinder Using a Direct Numerical Simulation, *Turbu-*

*lence in Complex Flows*, eds. P. Purtell and C. Wark, FED-V 203, 11-19.

Mittal, R., 1995. Study of flow past circular and elliptic cylinders using a direct numerical simulation, PhD Thesis, Univ. of Illinois at Urbana-Champaign.

Mittal, R. and Balachandar, S. , 1995a. Generation of Streamwise Vortical Structures in Bluff Body Wakes, *Phys. Rev. Lett.*, 75, No. 7, 1300-1303.

Mittal, R. and Balachandar, S., 1995b. Effect of Three-Dimensionality on the Lift and Drag of Nominally Two-Dimensional Cylinders, R. Mittal and S. Balachandar, *Phys. Fluids*, 7 (8), 1841-1865.

Mittal, R., and Balachandar, S. 1995c. Vortical structures in bluff body wakes. *AIAA 95-0867*.

Mittal, R. and Balachandar, S., 1996. Direct Numerical Simulation of Flow Past Elliptic Cylinders, *J. Comput. Phys*, 124, 351-367.

Moser, R. D., and Rogers, M. M. 1991. Mixing and transition to small scales in a plane mixing layer. *Phys. Fluids. A*, 3, 1128-1135.

Noack, B. R., König, M., and Eckelmann, H. 1993. Three-dimensional stability analysis of the periodic flow around a circular cylinder, *Phys. Fluids*, 5, 1279-1281.

Soria, J., and Cantwell, B. J. 1993. Identification and classification of topological structures in free shear flows. 379-390. *Eddy Structure Identification in Free Turbulent Shear Flows*, Bonnet, J. P., and Glauser, M. N., eds. Kluwer Academic Publishers, Netherlands.

Thompson, M., Hourigan, K., and Sheridan, J. 1996. Three-dimensional instabilities in the wake of a circular cylinder, *Exp. Therm. Fluid Sci.*, 12, 190-196.

Wieselsberger, C. 1922. New Data on the Laws of Fluid Resistance, *NACA TN 84*.

Williams, D.R., Mansy, H., and Abouel-Fotouh, A. 1996. Three-dimensional subharmonic waves during transition in the near-wake region of a cylinder, *Phys. Fluids* 8 (6), 1476-1485.

Williamson, C. H. K. 1991. Three-dimensional aspects and transition of a wake of a circular cylinder. *Seventh Turbulent Shear Flows*, Springer-Verlag, Berlin, 173-194.

Williamson, C.H.K. 1996. Vortex dynamics in the cylinder wake, *Ann. Rev. Fluid Mech.*, 28, 477-539.

Wu, J., Sheridan, J., Soria, J., and Welsh, M. C. 1994. An experimental investigation of the streamwise vortices in the wake of a bluff body. *J. Fluids Struct.*, 8, 621-635.

Zhang, H-Q, Fey, U., Noack, B. R., König, M., and Eckelmann, H. 1995. On the transition of the cylinder wake, *Phys. Fluids*, 7, 779-794.

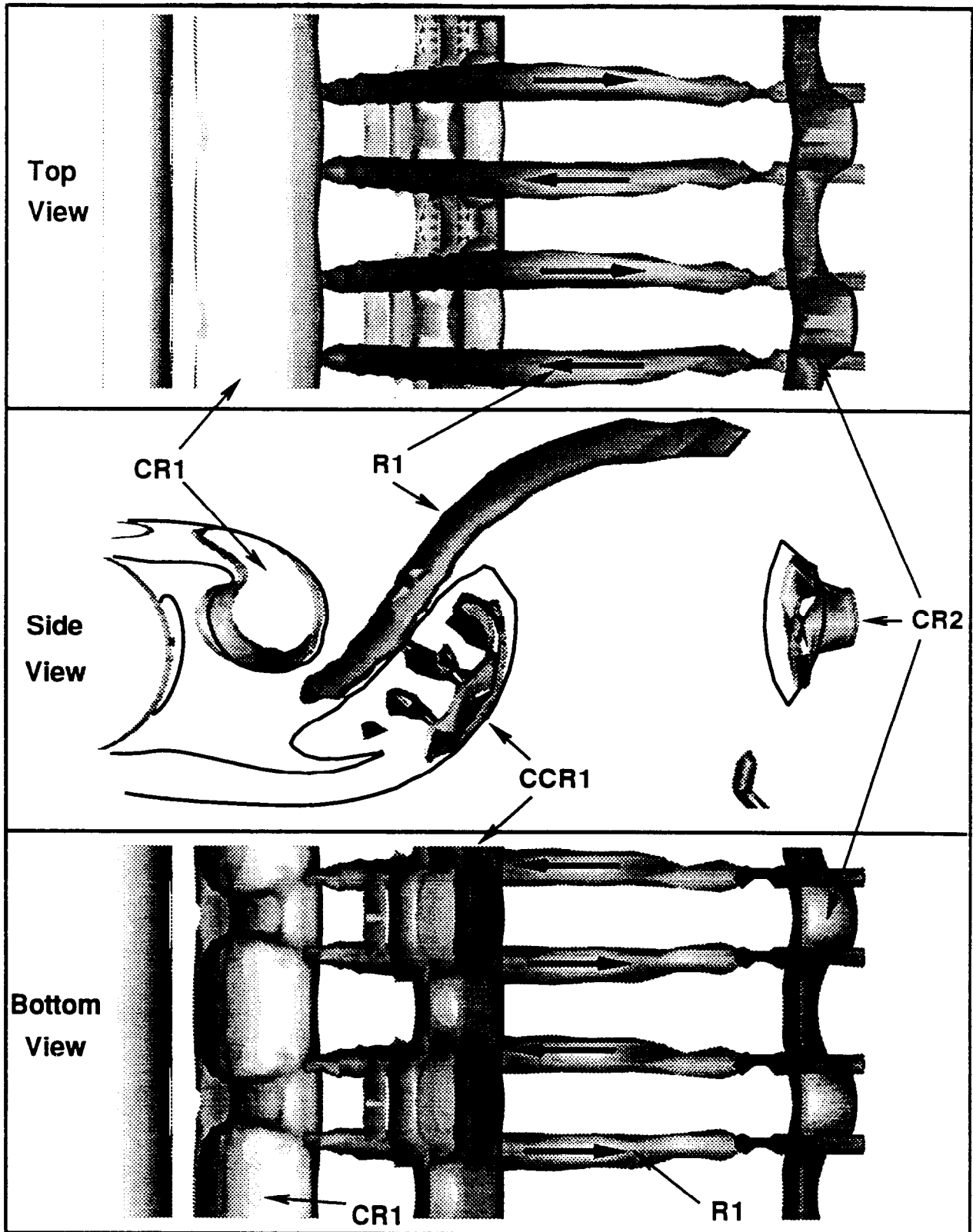


**Figure (2)** Top, side and bottom view of vortical structures in the near wake visualized in simulation 3DF. The flow is from left to right and the aft end of the cylinder is shown on the left side of the plots. Two contour lines of spanwise vorticity have also been plotted in the side view.

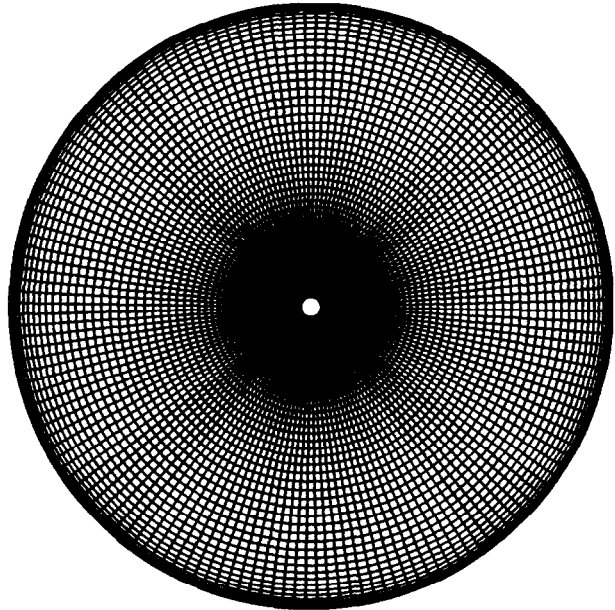


**Figure (1)** Axial view of the  $81 \times 160$  grid used in the present study.

Top View

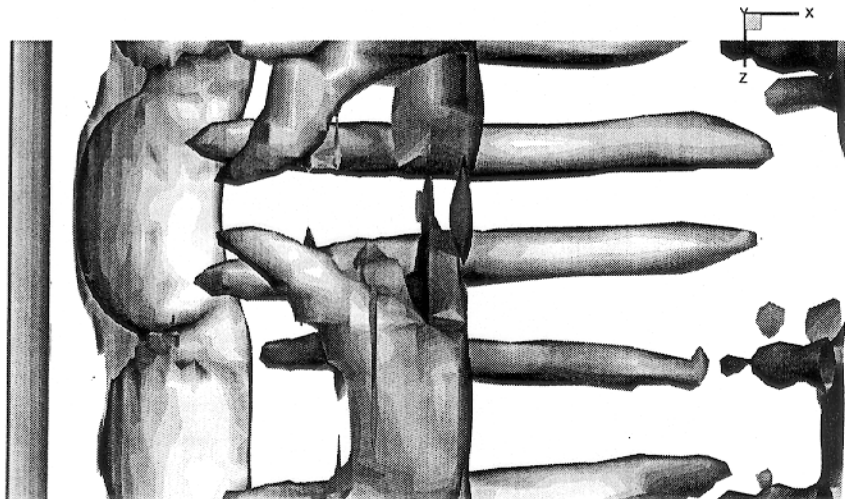


**Figure (3)** Top view of the vortical structure in the near wake visualized in simulation 3DFS. The flow is from left to right. Due to the effect of the subharmonic instability a horseshoe vortex can be observed in the near wake.

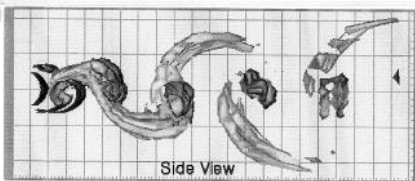
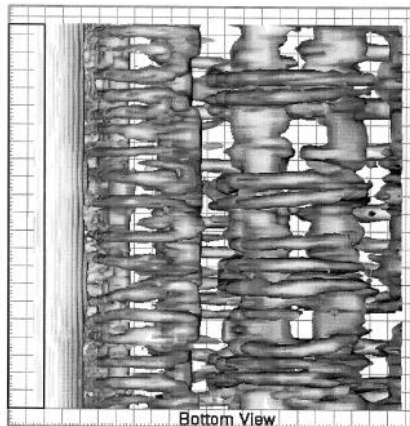
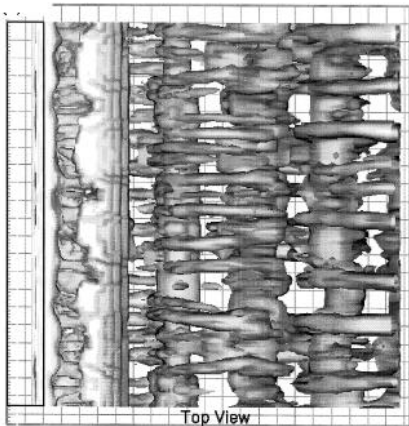


**Figure (4)** (a) Top, (b) side and (c) bottom view of the vortical structures in the near wake visualized in the simulation 3DA, with the a large span of  $12\lambda_c$ . The flow is from left to right.